ELSEVIER

Physica A 304 (2002) 23–42

PHYSICA A

www.elsevier.com/locate/physa

Models for a liquid–liquid phase transition

S.V. Buldyrev[a], G. Franzese[a], N. Giovambattista[a], G. Malescio[b], M.R. Sadr-Lahijany[a], A. Scala[a], A. Skibinsky[a], H.E. Stanley[a,*]

[a] *Center for Polymer Studies and Department of Physics, Boston University, Boston, MA 02215, USA*
[b] *Dipartimento di Fisica, Università di Messina and Istituto Nazionale Fisica della Materia, 98166 Messina, Italy*

Dedicated to Prof. S.-H. Chen on the occasion of his 65th birthday

Abstract

We use molecular dynamics simulations to study two- and three-dimensional models with the isotropic double-step potential which in addition to the hard core has a repulsive soft core of larger radius. Our results indicate that the presence of two characteristic repulsive distances (hard core and soft core) is sufficient to explain liquid anomalies and a liquid–liquid phase transition, but these two phenomena may occur independently. Thus liquid–liquid transitions may exist in systems like liquid metals, regardless of the presence of the density anomaly. For 2D, we propose a model with a specific set of hard core and soft core parameters, that qualitatively reproduces the phase diagram and anomalies of liquid water. We identify two solid phases: a square crystal (high density phase), and a triangular crystal (low density phase) and discuss the relation between the anomalies of liquid and the polymorphism of the solid. Similarly to real water, our 2D system may have the second critical point in the metastable liquid phase beyond the freezing line. In 3D, we find several sets of parameters for which two fluid–fluid phase transition lines exist: the first line between gas and liquid and the second line between high-density liquid (HDL) and low-density liquid (LDL). In all cases, the LDL phase shows no density anomaly in 3D. We relate the absence of the density anomaly with the positive slope of the LDL–HDL phase transition line.

PACS: 65.20.+w; 61.20.−p; 61.50.−f; 64.10.+h

Keywords: Liquid–liquid phase transition; Thermodynamic anomalies; Soft-core potential

* Corresponding author. Tel.: +1-617-3532617; fax: +1-617-3533783.
E-mail address: hes@bu.edu (H.E. Stanley).

0378-4371/02/$ - see front matter
PII: S0378-4371(01)00566-0

1. Introduction

Most liquids contract upon cooling and become more viscous with pressure. This is not the case for the most important liquid on earth, water. For at least 300 years it has been known that the specific volume of water at ambient pressure starts to increase when cooled below $T = 4^{\circ}\mathrm{C}$ [1]. It is perhaps less known that the viscosity of water decreases upon increasing pressure in a certain range of temperatures [2–4]. Moreover, in a certain range of pressures, water exhibits an anomalous increase of compressibility, and hence an increase of density fluctuations, upon cooling. These anomalies are not restricted to water but are also present in other liquids [5–7]. In mathematical terms, these anomalies can be expressed as follows. The thermal expansion coefficient is defined as

$$\alpha_P \equiv V^{-1}\left(\frac{\partial V}{\partial T}\right)_P , \tag{1}$$

where V, T and P are volume, temperature and pressure, respectively. If the density anomaly is present, α_P becomes negative for $T < T_\rho(P)$, so that equation $T = T_\rho(P)$ defines a line of maximum density, ρ, on the (P,T) plane.

At constant pressure, the isothermal compressibility

$$K_T \equiv -V^{-1}\left(\frac{\partial V}{\partial P}\right)_T \tag{2}$$

starts to increase if temperature decreases below $T < T_K(P)$. Thus $T = T_K(P)$ defines a line of minimum compressibility.

Finally, the coefficient of self-diffusion increases with pressure for $P < P_D(T)$. Accordingly, $P = P_D(T)$ defines a line of maximum diffusivity. This line coincides with the line of minimum viscosity, since viscosity is inversely proportional to the diffusion coefficient. The experimental phase diagram of water with the lines $T = T_\rho(P)$, $T = T_K(P)$, and $P = P_D(T)$ is shown in Fig. 1. The anomalies are present in the regions to the left from these lines. Below the freezing temperatures, the measurements were performed in the supercooled liquid state.

It is widely acknowledged that these anomalies are related to the hypothetical second critical point C_2 which may exist in the supercooled region of the water phase diagram. This critical point was first discovered by computer simulations of the ST2 potential, which has a strong built-in tetrahedral anisotropy. The simulations [8–10] predict that for real water the second critical point may occur at temperatures $T \approx 200\,\mathrm{K}$ and pressures $P \approx 150\,\mathrm{MPa}$. This region of the water phase diagram lies beyond the line of homogeneous nucleation and thus cannot be directly studied experimentally. Indirect evidence of the existence of the second critical point has been obtained by high-pressure melting experiments [11] and experimental studies of the structure of the supercooled water [12].

The existence of the two amorphous solids, high-density amorphous (HDA) ice and low-density amorphous (LDA) ice below the glass transition of 130 K yields another evidence [13] of the liquid–liquid phase transition at higher temperatures where the

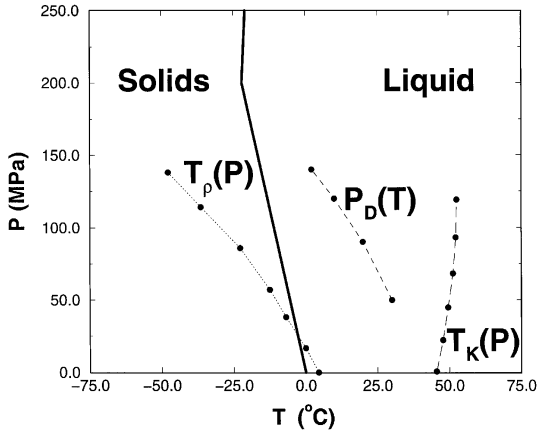

Fig. 1. Sketch of the phase diagram of water. The portion of the $T_\rho(P)$ line that is to the left of the melting line corresponds to experiments in the supercooled region of water. Notice that the presence of a density anomaly in the region of the negatively sloped melting line can occur in the metastable phase of the liquid. Data are obtained from Refs. [2–4].

amorphous phases quickly crystallize due to high molecular mobility. The extrapolation of the amorphous solids coexistence line above the glass transition seems to coincide with the putative liquid–liquid phase transition line estimated from the high pressure experiments and the extrapolation of the equation of state of liquid water below the homogeneous nucleation line.

While the first-order phase transition between two liquid phases has not been directly observed in water, it may be present in other substances. Recent experimental results [14] indicate that phosphorus, a single-component system, can have two liquid phases: a high-density liquid (HDL) and a low-density liquid (LDL) phase. A first-order transition between two liquids of different densities [5] is consistent with experimental data for a variety of materials [15,16], including single-component systems such as water [6,12,13,17], silica [18] and carbon [19]. Molecular dynamics simulations of very specific models with strong tetrahedral anisotropy for liquid carbon [20] and supercooled silica [21], beside supercooled water [5,8–10], predict a LDL–HDL critical point, but a coherent and general interpretation of the LDL–HDL transition is lacking.

We have shown that the presence of liquid anomalies [22–24] and the existence of the LDL–HDL phase transition [25] can both be directly related to an interaction potential [26] with an attractive part and two characteristic short-range repulsive distances (Fig. 2). The smallest of these two distances is associated with the hard core of the molecule, while the largest one is associated with the soft core. Although directional bonding is certainly a fundamental issue in obtaining quantitative predictions for network-forming liquids like water [27], it could be the case that isotropic spherically-symmetric core-softened potentials can be the simplest framework to understand the physics of the liquid–liquid phase transition and liquid state anomalies.

Soft-core potentials were first introduced by Stell, Hemmer, and their coworkers [28,29] in order to explain the isostructural solid–solid phase transition ending in a

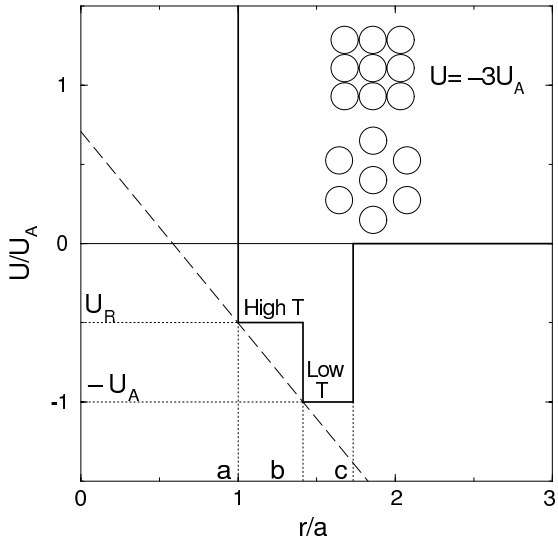

Fig. 2. The soft-core double-step potential used in two dimensions (2D) MD simulations and 1D analytical calculations: a is the hard-core distance, b the soft-core distance, c the attractive distance, U_R the (soft core) repulsive energy with respect to the attractive energy U_A. In 3D MD simulations we use a potential with $U_R > 0$. At low temperatures, the particles occupy the attractive well and do not penetrate into the soft core. At high temperatures, the particles can penetrate the soft core, and hence the average distance between particles may decrease—resulting in a density anomaly. The dashed line shows the Maxwell construction in 1D. The slope of this line gives the critical pressure at which two phases with specific volumes $v = a$ and b coexist at $T = 0$. The inset shows the two local structures in 2D simulations with the same potential energy per particle $U = -3U_A$.

second critical point. They also pointed out that for the 1D model with a long-range attractive tail, the isobaric thermal expansion coefficient, can take an anomalous negative value. Debenedetti et al., using general thermodynamic arguments, confirmed that a "softened core" can lead to $\alpha_P < 0$ [30]. Stillinger and collaborators found $\alpha_P < 0$ for a 3D system of particles interacting by purely repulsive interactions—a Gaussian potential [31–33].

Soft-core interactions are common in many single-component materials in the liquid state (in particular liquid metals [28,34–40,5]), and such potentials are often used to describe systems that exhibit a density anomaly [5]. Furthermore, ab initio calculation [34] and inversion of the experimental oxygen–oxygen radial distribution function [41,42] reveal that a "core-softened" potential can be considered a realistic first-order approximation for the interaction between water molecules (See Fig. 3). A similar potential was used to model water anomalies in one [22,23,43,44] and 2D [24,45]. A continuous potential of an analogous form models the interaction between clusters of strongly bonded pentamers of water [46].

Soft-core interactions (Fig. 2) qualitatively reproduce the density anomaly of water (Fig. 1). At sufficiently low pressures and temperatures, nearest-neighbor pairs are separated by a soft-core distance $r \approx b$ to minimize the energy. As temperature increases, the system explores a larger portion of the configurational space in order to gain more

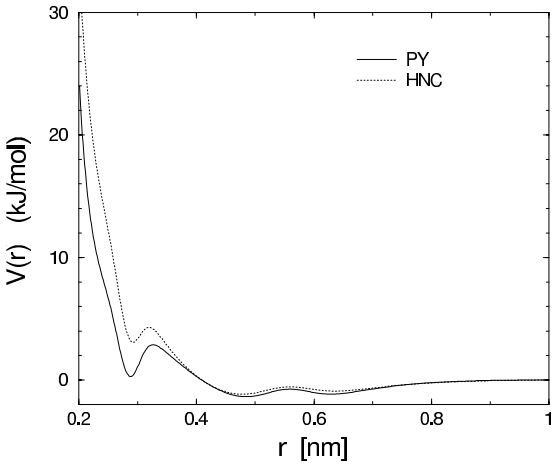

Fig. 3. The potentials derived by Head-Gordon and Stillinger from the Ornstein-Zernike equation using the Percus–Yevick (PY) and hypernetted chain (HNC) approximations from the experimental oxygen–oxygen pair correlation function at $T = 25^{\circ}$C for liquid water. Both approximations yield for $r < 0.4$ nm a repulsive soft core which is responsible for creating four nearest-neighbors local structure, imitating hydrogen bond network. The potential becomes strongly repulsive at distances smaller than 0.27 nm corresponding to the distance between oxygens in a pair of molecules linked by a hydrogen bond. This distance can be taken as a hard-core distance of the potential.

entropy. This includes the penetration of particles into the softened core, which can cause an anomalous contraction upon heating.

Several explanations have been developed to understand the liquid–liquid phase transition. For example, the *two-liquid model* [16] assumes that liquids at high pressure are a mixture of two liquid phases whose relative concentration depends on external parameters. Other explanations for the liquid–liquid phase transition assume an anisotropic potential [5,8,20,21]. We have seen [25] that liquid–liquid phase transition phenomena can arise solely from an isotropic pair interaction potential with two characteristic distances.

For molecular liquid phosphorus P_4 (as for water), a tetrahedral open structure is preferred at low pressures P and low temperatures T, while a denser structure is favored at high P and high T [14,6,17]. The existence of these two structures with different densities suggests a pair interaction with two characteristic distances. The first distance can be associated with the hard-core exclusion between two particles and the second distance with a weak repulsion (soft core), which can be overcome at large pressure. We used [25] a generic model composed of particles interacting via an isotropic soft-core pair potential (Fig. 2 with $U_R > 0$). Such isotropic potentials can be regarded as resulting from an average over the angular part of more realistic potentials, and are often used as a first approximation to understand the qualitative behavior of real systems [28,34–40,47,5]. For Ce and Cs, Stell and Hemmer proposed a potential with nearest-neighbor repulsion and a weak long-range attraction [28]. By means of an exact analysis in 1D, they found two critical points, with the high-density critical point interpreted as a solid–solid transition. Then analytic calculations [35], simulations [36] and exact solution in 1D [37] of the structure factor for a model with a soft-core

potential were found consistent with experimental structure factors for liquid metals such as Bi. The structure factor was also the focus of a theoretical study of a family of soft-core potentials, for liquid metals, by means of mean-spherical approximation [38]. More recently, the analysis of the solid phase of a model with a soft-core potential [39] was related to the experimental evidence of a liquid–liquid critical point in the K_2Cs metallic alloy [40].

Recently, 3D molecular dynamic simulations of Franzese et al. [25] show that this class of potentials can reproduce the existence of the second critical point in the liquid phase. They also show that the LDL and HDL phases can occur in systems with no density anomaly. In contrast, 2D simulations [22,24] show density anomalies in the liquid phase but no second critical point, which may be hidden—as in real water—beyond the homogeneous nucleation line.

Jagla used Monte Carlo simulations of the potentials with an impenetrable hard core a, a soft core represented by a linear repulsive ramp with negative slope and a linear attractive ramp with positive slope. He reproduced density anomalies simultaneously with HDL–LDL phase transition in two- and three-dimensions. He also reproduced the LDA–HDA transition below the glass-transition temperature [45].

All the above results suggest that the soft-core spherically symmetric potentials provides a generic explanation for both LDL–LDH phase transitions and for liquid phase anomalies, but these phenomena may not necessarily occur simultaneously. Here, we review the results [22–25] on the double-step soft-core potentials.

2. One-dimensional model

The double-step potentials that we study are shown in Fig. 2 as a function $U(r)$ of particle pair distance r. This potential is composed of a hard core of diameter a, a shoulder of width $b-a$ with a constant value U_R repulsive with respect to an attractive well of width $c-b$ and depth $-U_A<0$.

In 1D, the average interparticle distance r coincides with the specific volume v, and thus the dependence of the free energy $F(v,T)=U(v,S)-TS$ coincides at $T=0$ with pair potential $U(v)$. Indeed, at $T=0$, the entropy S is also equal to zero, which means that there is no disorder in the system and all interparticle distances are equal to v. Furthermore, if $c<2a$, only pairs of neighboring particles interact with each other and thus the total potential energy per particle coincides with pair potential $U(v)$. Making Maxwell construction (see Fig. 2), one can see that at $T=0$, the specific volume of the system has a discontinuity at pressure $P=P_{C_2}=(U_R+U_A)/(b-a)$ changing its value from $v=a$ above P_{C_2} to $v=b$ below P_{C_2}. Although one dimensional system cannot have phase transitions at positive temperatures, the points $(T=0,P=0)$ and $(T=0,P=P_{C_2})$ can be regarded, respectively, as a normal liquid–gas critical point and an additional second critical point between a high density phase and a low density phase.

If $c<2a$, one can factorize the partition function $Z(T,P)$ for 1D system [24],

$$Z(T,P)\sim\Omega(T,P)^N\,,$$

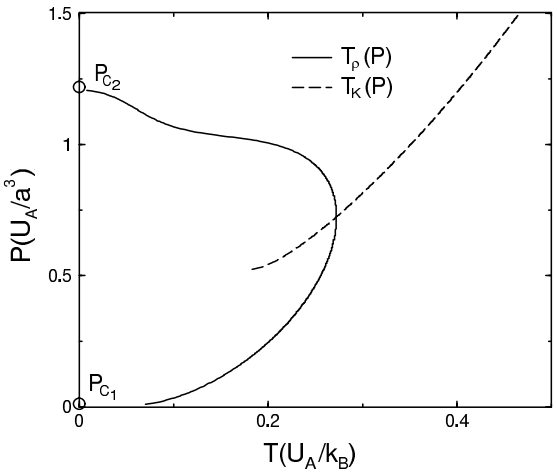

Fig. 4. The density maximum line (solid line) and compressibility maximum line (dashed line) computed for a 1D system using Eq. (3) and a set of parameters used in 2D simulations: $b=\sqrt{2}a$, $c=\sqrt{3}a$, $U_R/U_A=-0.5$. Note that the two lines intersect at the point of maximum temperature on the density maximum line.

where N is the number of particles, k_B is Boltzmann constant, and

$$\Omega(T,P)=\int_0^\infty \exp\left(-\frac{Pr+U(r)}{k_BT}\right)\,\mathrm{d}r\,.$$

Differentiation of the Gibbs potential $G(T,P)=-k_BT\ln Z(T,P)$ with respect to P yields a close form for the equation of state

$$v\equiv V/N=k_BT\frac{\partial\ln\Omega}{\partial P}\,. \tag{3}$$

Fig. 4 reproduces the density maximum and compressibility minimum values computed according to Eq. (3) for a specific set of parameters of the potential. Note that at a certain value of P the maximum density temperature $T_\rho(P)$ reaches its maximum temperature, at which $\mathrm{d}T_\rho/\mathrm{d}P=0$. This feature was observed in simulations with SPC/E and ST2 potentials [9,10]. This maximum in $T_\rho(P)$ can be a general phenomenon stemming from the core-softened type of potential. Extrapolation of the $T_\rho(P)$ line on the experimental water phase diagram to negative pressures suggests that this maximum may exist in stretched water. Another feature of this maximum is that it lies on the line of compressibility minima, i.e., the $T_K(P)$ and $T_\rho(P)$ lines always cross when $\mathrm{d}T_\rho/\mathrm{d}P=0$. This is a pure mathematical consequence [48] of the existence of the double partial derivatives of the equation of state $V=V(P,T)$ with respect to P and T.

3. Two-dimensional model

In 2D, the analytic solution is impossible, thus we determine the equation of state and diffusion coefficient using molecular dynamic simulations. Since molecular dynamic

simulations are time-consuming, it is important to select a priori a set of parameters which yields the density anomaly in the liquid state. In 2D, a system with a square well potential easily crystallizes at low temperatures into a triangular crystal for $c < \sqrt{2}a$, into a square crystal for $\sqrt{2}a < c < \sqrt{3}a$, and again into triangular crystal for $c > \sqrt{3}a$ [49]. Keeping in mind the explanation of the density anomaly in terms of two local crystal-like structures, we select the parameters of the double step potential to be $b = \sqrt{2}a$, $c = \sqrt{3}a$, $U_R/U_A = -0.5$. For this set of parameters, both a high density square crystal and a lower density triangular crystal have the same potential energies per particle $U = -2U_A + 2U_R = -3U_A$, and we can expect that the system is frustrated in the liquid state, in which local structures resemble either a square or a triangular crystal (Fig. 2).

In order to simulate the double step potential shown in Fig. 2, we use MD simulations based on the quick sorting of the table of collision times [50–53]. Between collisions, the particles move along straight lines at a constant velocity. Whenever the hard cores, soft cores, or attractive wells collide, the velocities of the molecules instantly change, and the total energy, momentum, and angular momentum are conserved. This type of MD simulation proves to be useful in many diverse problems [54], e.g., the formation of quasi-crystals [49], protein folding [55] and glass transitions [56,57].

We simulate, for a system of $N = 896$ disks of radius $a/2$, state points along constant-volume paths [24]. The average pressure is calculated using the virial equation for step potentials [50]. For thermalization, we use the Berendsen method of rescaling the kinetic energy [50,58]. We thermalize the system for 10^5 time units, which corresponds to $\sim 10^6$ collisions per particle, and then acquire data for 10^6 time units corresponding to $\sim 10^7$ collisions per particle.

3.1. Density anomaly

Fig. 5 shows a set of different isochores on the $(P-T)$ plane obtained in our simulations. Fig. 6 shows snapshots of the system at different points on the phase diagram. Note that the region of negative pressures corresponds to a metastable stretched liquid, which exists above the liquid–gas spinodal. In simulations, negative pressure appears due to periodic boundary conditions: the stretched liquid tries to contract the surface of a torus on which it is simulated. For the densities below the spinodal density, the liquid breaks and the voids of gaseous phase appear in the simulation. As soon as voids appear, the negative pressure drops and becomes close to zero. We make sure that no voids appear for the densities $\rho > 0.513a^{-3}$. In addition to the isochores, we show the gas–liquid equilibrium line which is obtained by measuring gas pressure in a system consisted of a large liquid droplet surrounded by gas. The equation of the equilibrium line approximately satisfies Arrhenius law: $P(T) = P_0 \exp(-H/k_B T)$, where $H = 3.165U_A$, $P_0 = 7.55U_A/a^3$. The phase transition ends at a critical point C_1 with $T_{C_1} = 0.5265U_A/k_B$, $P_{C_1} = 0.02U_A/a^3$, $\rho_{C_1} = 0.335a^{-3}$, which we find by identifying an isotherm with an inflection point, that separates the monotonic isotherms from the non-monotonic isotherms [5].

To confirm that we are investigating the liquid state part of the phase diagram, we introduce a criterion to distinguish the liquid state from a frozen state. We

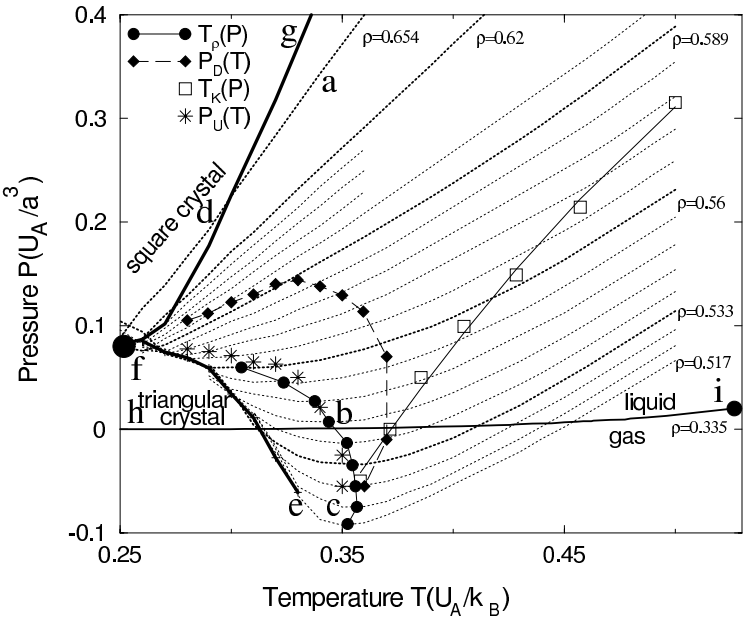

Fig. 5. Isochores for a 2D system (dotted lines) together with crystallization lines (heavy line), and a liquid–gas equilibrium line (solid line ending at the critical point). The density maximum line $T_\rho(P)$, compressibility maximum line $T_K(P)$, diffusivity maximum line $P_D(T)$, and potential energy maximum line $P_U(T)$ are shown by symbols indicated in the figure. The letters indicate the points on the phase diagram corresponding to the snapshots on Fig. 6. The large circle at $T = 0.25U_A/k_B$, $P = 0.075U_A/a^3$ indicates the hypothetical position of the second critical point. Density ρ is measured in a^{-3} units.

determine the freezing line as the location of points where isochores overlap. In this way, we establish an approximate location for the freezing line. Crossing this line from the liquid side, we find a sharp decrease in diffusivity D coinciding with the appearance of slowly-decaying peaks in $g(r)$ as a function of r, which signals the build up of long-range correlations (Fig. 7), which is a characteristic of 2D solids.

The temperature of the density maximum $T = T_\rho(P)$ line is the border of the region in the $P - T$ plane where the liquid expands upon cooling. The T_ρ line corresponds to the set of minima along the isochores. Indeed, due to well known thermodynamic relation, $(\partial P/\partial T)_V = \alpha_P/K_T$ [31–33]. Therefore, the region in the (P–T) plane with negative α_P corresponds to the region of negative $(\partial P/\partial T)_V$. Moreover, at density maximum, where $\alpha_P = 0$, the pressure has its minimum $(\partial P/\partial T)_V = 0$. Note that, as in case of 1D system, the $T_\rho(P)$ line has a maximum temperature. But now this maximum is at negative pressure $P_m < 0$, as in computer simulations of realistic water potentials.

3.2. Other anomalies

We find isothermal compressibility by differentiation of the numerical values $V = V(P,T)$, found in the simulations. As expected, the compressibility minima line $T_K(P)$ crosses the $T_\rho(P)$ line at the point of its maximum temperature $P_m < 0$.

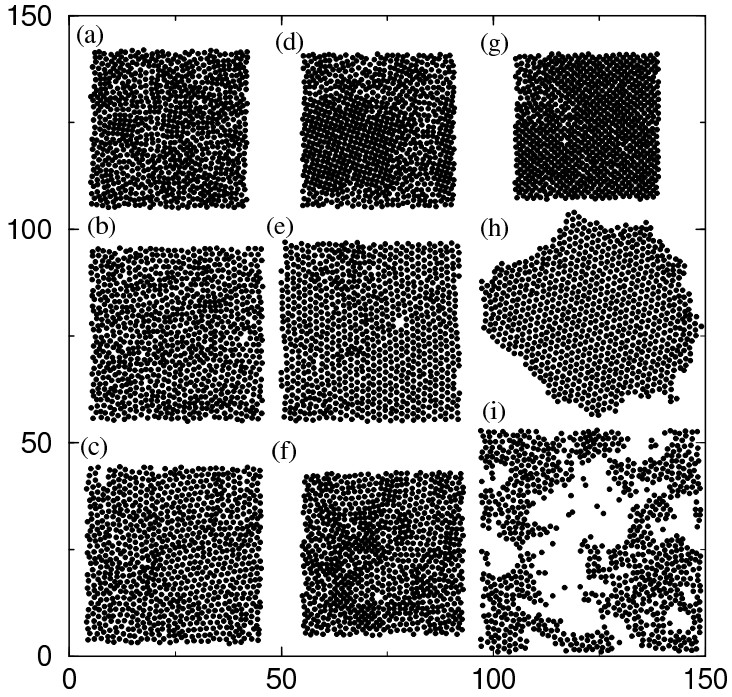

Fig. 6. A series of snapshots of the 2D system at various points on the phase diagram. (a) The high-pressure liquid phase near the point of square crystal formation; many local structures resembling square crystals are present. (b) The liquid phase near the temperature maximum density line; both high-density square and low-density triangular local structures are abundant. (c) The liquid phase near triangular crystal formation; large local structures resembling triangular crystals are present. (d) The liquid phase coexisting with the square crystal phase. (e) The liquid phase coexisting with the triangular crystal phase. (f) The liquid phase near the second critical point. (g) The square crystal phase. (h) The triangular crystal phase coexisting the gas phase. (i) The fluid in the vicinity of the liquid–gas critical point.

The density anomaly is also related to the anomalous decrease of entropy during isothermal expansion. Indeed $(\partial P/\partial T)_V = -\partial^2 F/\partial T\partial V = (\partial S/\partial V)_T$. Thus the region of the density anomaly where $(\partial P/\partial T)_V < 0$, coincides with the region of entropy anomaly, where $(\partial S/\partial V)_T < 0$. Therefore, at constant T, entropy increases with pressure and reaches its maximum at pressure $P_S(T)$. The line $P_S(T)$ coincides with the line $T_\rho(P)$. Independent calculation of entropy by thermodynamic integration

$$S = \int \frac{\mathrm{d}U + P\,\mathrm{d}V}{T}$$

along the isochores and isotherms confirms this conclusion for our simulations.

Furthermore, the line of maximum density is closely related to the line of maximal potential energy. Indeed due the first and the second laws of thermodynamics, $T(\partial S/\partial V)_T = (\partial U/\partial V)_T + P$. Hence in the region of density anomaly with $P > 0$, potential energy must increase with contraction $(\partial U/\partial V)_T < -P < 0$ until it reaches its maximum at a higher pressure $P_U(T) > P_S(T)$. This line is also presented in Fig. 5.

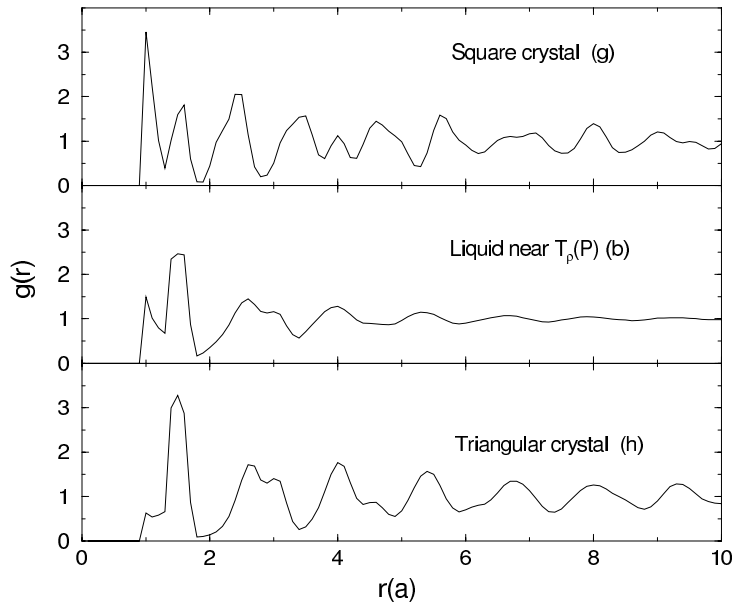

Fig. 7. Radial density correlation functions computed for points b, g, and h on the phase diagram (Figs. 5 and 6). The peak at $r = 1.5$ corresponds to the open triangular crystal structure. The peak at $r = 1.0$ corresponds to the closed square crystal structure.

3.3. Structures in the liquid and solid phases

We see that the T_ρ line is located in the region of pressures where the freezing line is negatively sloped, as in water. A density anomaly and a negatively-sloped melting line are often associated [5,59]. This has proven to be the case for substances like water (Fig. 1) and tellurium [7] and for computer models [22,60]. This association is plausible since the isobaric thermal expansion coefficient α_P is related to the cross fluctuations in volume and entropy as

$$\alpha_P \equiv \frac{1}{k_B T V}\langle \delta V \ \delta S \rangle \,. \tag{4}$$

Approaching a freezing line, we expect local density fluctuations to have structures similar to the neighboring solid as they are going to trigger the liquid–solid transition. On the other hand, the Clausius–Clapeyron relation for the slope of the freezing line

$$\frac{\mathrm{d}P}{\mathrm{d}T} = \frac{\Delta S}{\Delta V} \tag{5}$$

implies that, if the freezing line is negatively sloped, the solid, which has a lower entropy than the liquid, will have a higher specific volume. Therefore, if the fluctuations in the liquid are "solid-like", α_P [Eq. (4)] will turn out to be negative.

To distinguish different local structures in the liquid, we plot the radial distribution function $g(r)$ for different pressures and temperatures (Fig. 7). At low pressures, as expected, cooling expels particles from the core, while increasing pressure at fixed temperature has the opposite effect.

Since our system is 2D, we can use visual inspection to develop an intuitive picture of the possible local structures (Fig. 6a–c). If the fluctuations in the liquid are "solid-like", near the freezing line we expect to see local structures that resemble the structure of the nearby solid.

We find that at low P and T, the system is frozen with a hexagonal structure (Fig. 6h). A "snapshot" of the system at low pressure (Fig. 6c) shows clearly that local patches with hexagonal order are present in the liquid phase near the freezing line. We will refer to this structure as the "open structure". Similarly, at high pressures the local patches in the liquid phase near the freezing line (Fig. 6a) resemble the structure of the system when it is frozen at low T and high P (Fig. 6g). We will refer to this as the "dense structure". (See Fig. 2). The radial correlation function for any point in the liquid state can be well approximated by a linear combination of radial correlation functions for open and close structures as in experimental studies of Ricci and Soper [17] (Fig. 7).

3.4. Diffusion anomaly

We next study the diffusion anomaly, which is another surprising feature of water. While for most materials diffusivity decreases with pressure, liquid water has an opposite behavior in a large region of the phase diagram [2–4] (Fig. 1).

We observe that our core-softened potential reproduces this anomaly. We first measure the mean square displacement $\langle \Delta r^2(t) \rangle \equiv \langle [r(t+t_0)-r(t_0)]^2 \rangle$ and then the diffusion coefficient using the relation

$$D = \frac{1}{2d} \lim_{t\to\infty} \frac{\langle \Delta r^2(t) \rangle}{t} \,. \tag{6}$$

We find that there is a region of the phase diagram in which D increases upon increasing P (Fig. 8).

In order to understand the diffusion anomaly, we first note that, for normal liquids, D decreases with P because upon increasing P the density increases and molecules are more constrained. In the case of water, the anomaly can be related to the fact that increasing pressure (and hence density) breaks hydrogen bonds, which in turn increases the mobility of the molecules. We present a more general explanation which can equally apply to our radially symmetric core-softened interaction which does not possess any directional bonds similar to hydrogen bonds. The low energy inter-particle state at $r \approx b$ plays the role of non-directional bond. Note that D is proportional to the mean free path of particles, which increases with the free volume per particle $v_{free} \equiv v - v_{ex}$, where v_{ex} is the excluded volume per particle resulting from the effective hard core. At low temperatures, v_{ex} for the dense structure is proportional to the area a^2 of the hard core, while for the open structure it is proportional to the area b^2 of the soft core. Increasing P decreases v, which is the main effect in normal liquids. For the core-softened liquid, on the other hand, increasing P can also decrease v_{ex} by transforming some of local open structures to dense structures. Since both Δv and Δv_{ex} decrease with P and since $\Delta v_{free} = \Delta v - \Delta v_{ex}$, the effect of P on D depends on whether Δv or Δv_{ex} dominates.

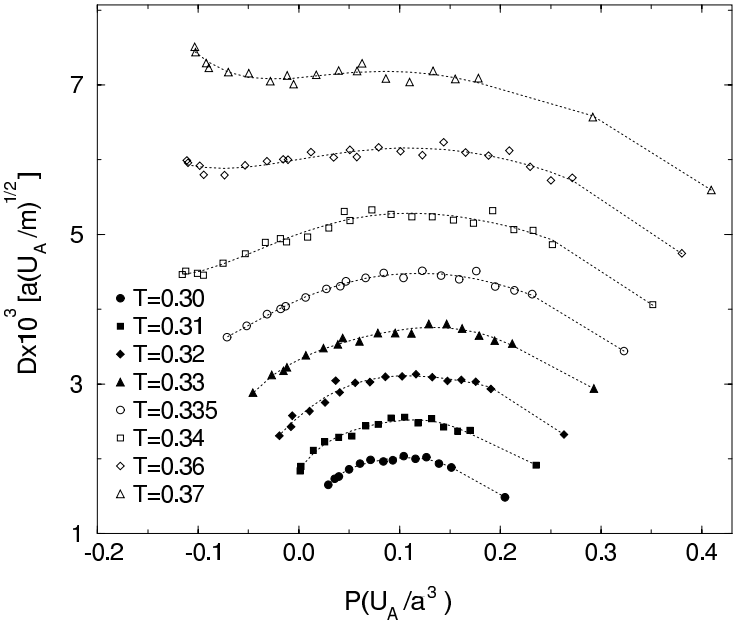

Fig. 8. Diffusion coefficient D in the liquid phase along various isotherms. Lines are intended as a guide for the eye. Notice the anomalous sections of the graph, where $(\partial D/\partial P)_T > 0$. Tempertures T are measured in U_A/k_B units. By choice m is the unitary mass.

The anomalous increase in D along the isotherms near the freezing line is a sign of the dominance of the Δv_{ex} term. The anomaly in D must disappear near a certain pressure above which the average distance between particles corresponds to the dense structure, and as a result the contribution of the open structure to v_{ex} is negligible.

Another explanation of the diffusivity anomaly can be obtained using the Adam–Gibbs relation $D \sim \exp(-A/TS_{conf})$, where S_{conf} is the configurational part of the entropy, and A is some positive constant [56,57,61,62]. Thus the diffusivity maximum must coincide with the maximum of configurational entropy. Since one can expect $S_{conf} \approx S$, the diffusivity maximum line must be located in the vicinity of the entropy maximum line $P_S(T)$, which coincides with the line of maximum density $T_\rho(P)$.

To test this prediction, we directly compute $S_{conf} = S - S_{vib}$, where S_{vib} is the vibrational part of the entropy. We find S by thermodynamic integration. We assume that $S_{vib} = -Nk_B \int \rho(x,y) \ln \rho(x,y)\, dx\, dy$, where $\rho(x,y)$ is the probability density of a particle when it is vibrating in a "cage" made up of surrounding nearest neighbors [49]. This is similar in spirit to finding the vibrational entropy by calculating the properties of the basins on a potential energy surface [61]. To implement the basins in discrete molecular dynamics, we replace the attractive well between b and c with a permanent bond of infinitely high energy, as in the simulation of polymers [55].

Since S_{vib} is proportional to the logarithm of the volume of the cage we have

$$\frac{\partial S_{conf}}{\partial V} = \frac{\partial S}{\partial V} - \frac{Nk_B}{v_{cage}} \frac{\partial v_{cage}}{\partial V}\,. \tag{7}$$

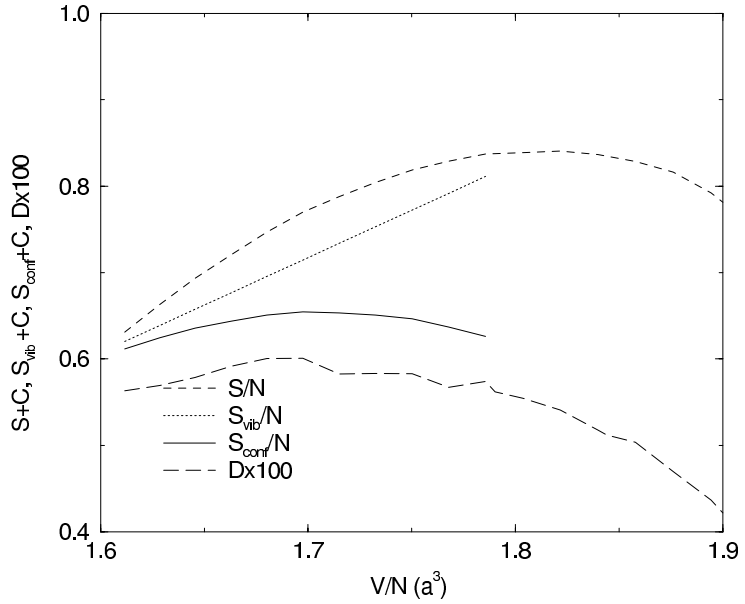

Fig. 9. The graphs of entropies S, S_{conf}, S_{vib}, and diffusion coefficient D versus specific volume V/N for $T = 0.33U_A/k_B$. The values of the entropies are shifted by different additive constants, which do not affect the positions of maxima. One can see that the positions of the maxima of the diffusion coefficient, coincide with the maximum of the configurational entropy.

One may expect that the volume of the cage decreases together with the volume of the system,

$$\frac{\partial v_{cage}}{\partial V} > 0\,.$$

Thus the maximum of configurational entropy must be achieved when

$$\frac{\partial S}{\partial V} = \frac{Nk_B}{v_{cage}}\frac{\partial v_{cage}}{\partial V} > 0\,,$$

i.e., at a higher pressure $P_{sc} > P_S(T)$, when the entropy and density anomalies already disappear. Our numerical calculations confirm that the line $P_D(T)$ coincides with the line of configurational entropy maxima $P_{sc}(T)$. The example of our calculation is shown on Fig. 9.

3.5. Second critical point

In summary the phase diagram (Fig. 5) of the simulated two dimensional system with isotropic hard soft-core potential (Fig. 2) qualitatively reproduces all the features of the experimental water phase diagram. As in real water, we did not find any second critical point in the liquid phase. Extrapolation of the isobars beyond the freezing line, show that they cross in a wide region of $T \approx 0.25U_A/k_B$, $P \approx 0.075U_A/a^3$. The region of the isobars crossing is related to the spinodal lines $(\partial P/\partial V)_T = 0$, which must originate at the hypothetical critical point C_2. The snapshot of the system shortly

after it has been quenched at the vicinity of this point so that it does not have time to crystallize is shown on Fig. 6f. One can see large clusters of high a low density phases, resembling the clusters of gaseous and liquid phases near regular critical point (Fig. 6i).

4. Three dimensional simulations

We attempted to find second critical point in 3D simulations [25]. To select the parameters for the molecular dynamics (MD) simulations is not easy, and MD is too time consuming to study a wide range of parameter values. The set of parameters used in 2D simulations does not produce in 3D neither density anomaly nor a liquid–liquid phase transition. Hence, we first solve the integral equation for $g(r)$ in the hypernetted chain approximation [63], whose predictions we can calculate very rapidly and efficiently. In the temperature–density (T–ρ) phase diagram, the region where the HNC approximation has no solutions is related [63] to the region where the system separates in two fluid phases. Thus this technique allows us to estimate the parameter range where two critical points occur, and hence to find useful parameters values for the MD simulations: $b/a = 2.0$, $c/a = 2.2$ and $U_R/U_A = 0.5$. We also use in the MD calculations several additional parameter sets. Note that, in contrast to 2D, in 3D the value of U_R should be positive.

Specifically we perform discrete MD simulations, described above, in 3D at constant volume V and number of particles N=490 and 850. We find, for each set of parameters, the appearance of two critical points (Fig. 10).

A critical point is revealed by the presence of a region, in the P–ρ phase diagram, with negative-slope isotherms. In MD simulations this region is related to the coexistence of two phases [5]. The (local) maximum and minimum along an isotherm correspond to the limits of stability of the existence of each single phase (supercooled and superheated phase, respectively). By definition, these maxima and minima are points on the *spinodal line* for that temperature. Since the spinodal line has a maximum at a critical point, a way to locate a critical point is to find this maximum. In our simulations (Fig. 10), we find two regions with negatively-sloped isotherms and the overall shape of the spinodal line has two maxima, showing the presence of *two* critical points, C_1 and C_2. Using the Maxwell construction in the P–V plane [5], we evaluate the *coexistence lines* of the two fluid phases associated with each critical point (Fig. 11). We estimate the low-density critical point C_1 at $T_1 = 0.606 \pm 0.004 U_A/k_B$, $P_1 = 0.0177 \pm 0.0008 U_A/a^3$, $\rho_1 = 0.11 \pm 0.01 a^{-3}$ and the high-density critical point C_2 at $T_2 = 0.665 \pm 0.005 U_A/k_B$, $P_2 = 0.10 \pm 0.01 U_A/a^3$, $\rho_2 = 0.32 \pm 0.03 a^{-3}$. Critical point C_1 is at the end of the phase transition line separating the gas phase and the LDL phase, while critical point C_2 is at the end of the phase transition line separating the gas phase and the HDL phase. Their relative positions resemble the phosphorus phase diagram, except that, in the experiments, C_2 has not been located [14], but is expected at the end of the gas-HDL transition line.

For phosphorus, the liquid–liquid transition occurs in the stable fluid regime [14]. In contrast, for our model, it occurs in the metastable fluid regime (see Fig. 10). To

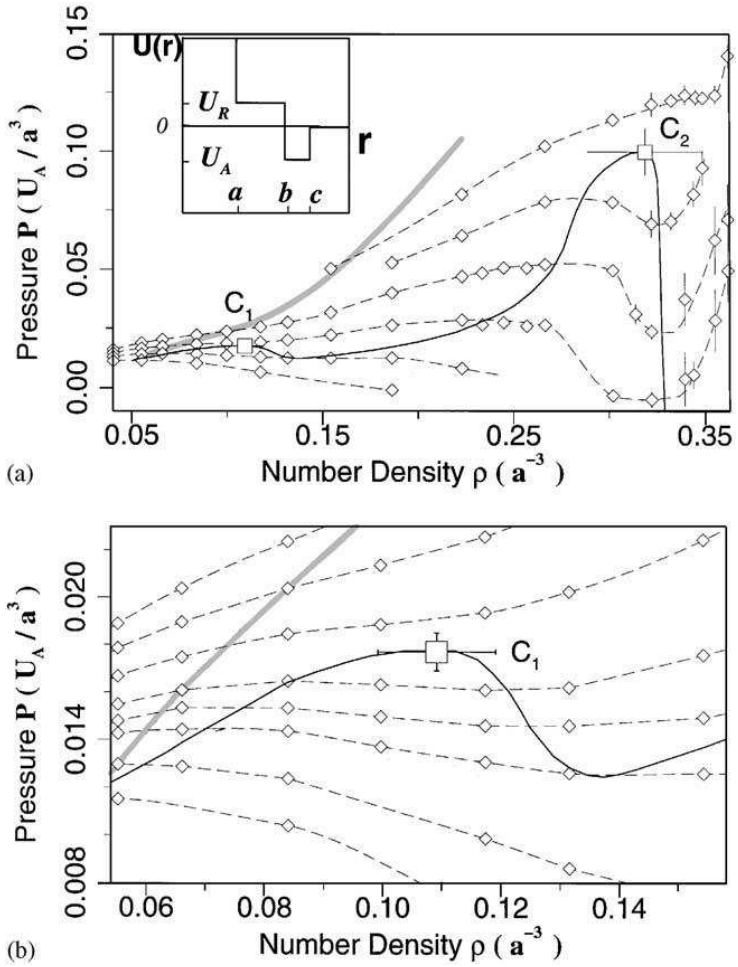

Fig. 10. Pressure–density isotherms, crystallization line and spinodal line from the MD simulations for the isotropic pair potential in 3D. (a), Inset: The pair potential energy $U(r)$ as a function of the distance r between two particles. (a) Several isotherms for (bottom to top) $k_BT/U_A = 0.57$, 0.59, 0.61, 0.63, 0.65, 0.67. Diamonds represent data points and lines are guides for the eyes. The solid line connecting local maxima and minima along the isotherms represents the *spinodal line*. The two maxima of the spinodal line (squares) represent the two critical points C_1 and C_2. (b) Enlarged view of the region around the gas-LDL critical point C_1 for $k_BT/U_A = 0.570$, 0.580, 0.590, 0.595, 0.600, 0.610, 0.620, 0.630.

determine the crystallization line we place a crystal seed, prepared at very low T, in contact with the fluid, and check, for each (T,ρ), if the seed grows or melts after 10^6 MD steps. The spontaneous formation (*nucleation*) of the crystal is observed, within our simulation times ($\approx 10^5$ MD steps), only for $\rho \geqslant 0.27a^{-3}$. We use the structure factor $S(Q)$—the Fourier transform of the density-density correlation function for wave vectors Q—to determine when the nucleation occurs. Indeed, at the onset of nucleation, $S(Q)$ develops large peaks at finite Q ($Q = 12a^{-1}$ and $Q = 6a^{-1}$). For each ρ, we quench the system from a high-T configuration. After a transient time for the fluid equilibration, we compute $P(T,\rho)$, averaging over 10^5–10^6 configurations generated from up to 12 independent quenches, making sure that the calculations are done before nucleation takes place.

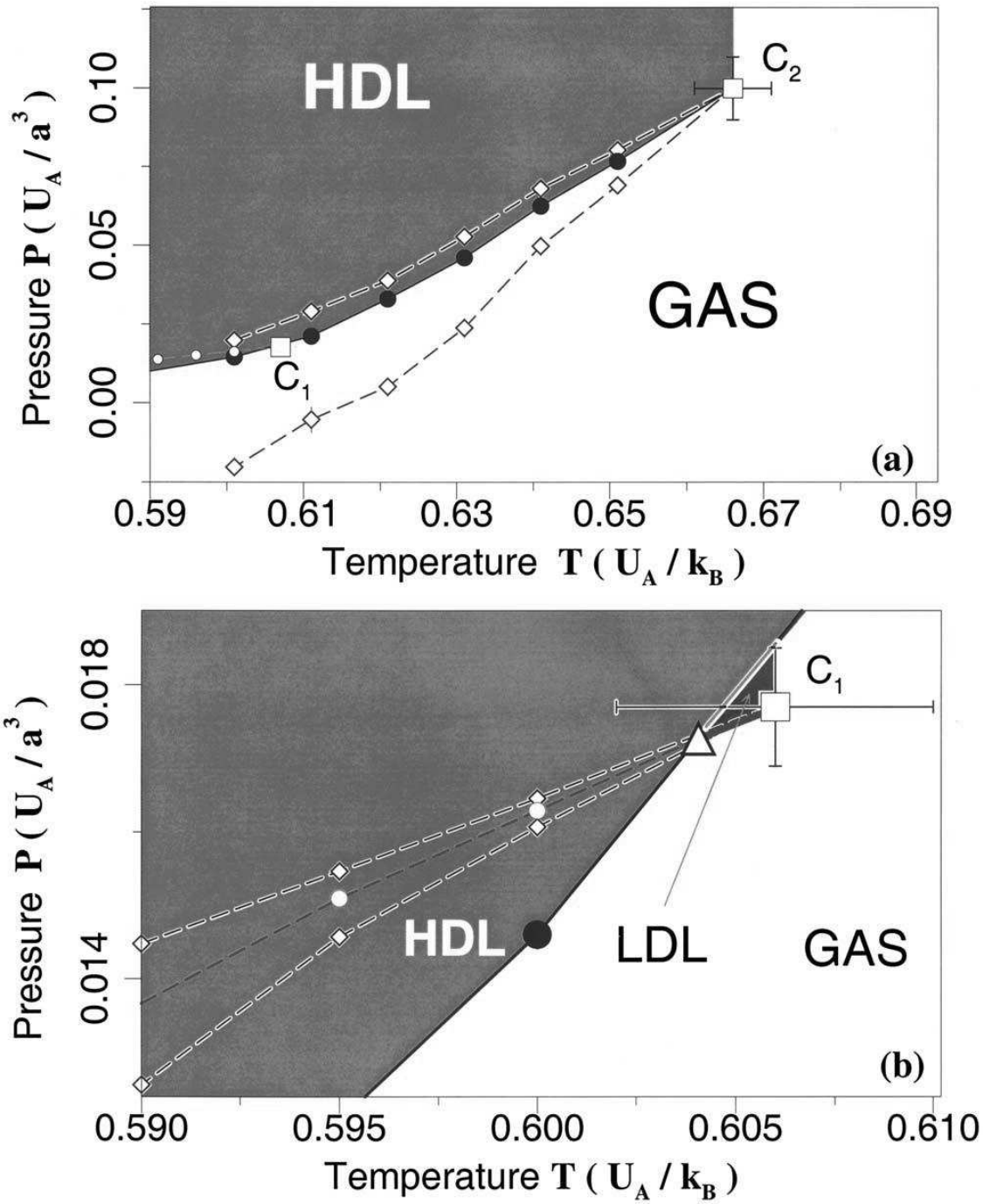

Fig. 11. The pressure-temperature phase diagram, with coexistence lines and critical points resulting from MD simulations. Panel (b) is a blow up of panel (a) in the vicinity of C_1. Circles represent points on the coexistence lines: open circles are for the gas-LDL coexistence, filled circles for the gas-HDL coexistence. Lines are guides for the eyes. The solid black line is the gas-HDL coexistence line. The red line is the gas-LDL coexistence line. The solid red line is stable, while the dashed red line is metastable, with respect to the HDL phase. The orange line is the LDL–HDL coexistence line. The triangle represents the *triple point*. The projection of the spinodal line is represented in (a) and (b) by diamonds with dashed lines. The spinodal line is folded in this projection, with two cusps corresponding to the two maxima in Fig. 10. Critical points occur where the coexistence lines meet these cusps. The critical point C_1 is for the gas-LDL transition, and C_2 is for the gas-HDL transition.

We therefore wish to understand how to enhance the stability of the critical points with respect to the crystal phase. We find that by increasing the attractive well width $(c-b)/a$, both critical temperatures T_1 and T_2 increase, and hence both critical points move toward the stable fluid phase, analogous to results for attractive potentials with a single critical point [64,65]. For example, for attractive well width $(c-b)/a=0.2$, both C_1 and C_2 are *metastable* with respect to the crystal, while for $(c-b)/a>0.7$ we find C_1 in the *stable* fluid phase.

The phase diagram depends sensitively also on the relative width of the shoulder b/a and on its relative height U_R/U_A. By decreasing b/a or by increasing U_R/U_A, T_2 decreases and becomes smaller than T_1. This means that, in these cases, the high-density C_2 occurs below the temperature of the gas–liquid critical point, i.e., C_2 is in the liquid phase and represents a LDL–HDL critical point, as in supercooled water [6,8,12].

The soft-core potential with the sets of parameter we use displays no "density anomaly" $(\partial V/\partial T)_P<0$. This result is at first sight surprising since soft-core potentials have often been used to explain the density anomaly (see, e.g., Section 3b and Refs. [5,22]). To understand this result, we consider the entropy S and the thermodynamic relation $-(\partial V/\partial T)_P=(\partial S/\partial P)_T=(\partial S/\partial V)_T(\partial V/\partial P)_T$. Since of necessity $(\partial V/\partial P)_T<0$, $(\partial V/\partial T)_P<0$ implies $(\partial S/\partial V)_T<0$, i.e., the density anomaly implies that the disorder in the system increases for decreasing volume. For example, this is the case for water.

For our system, we expect the reverse: $(\partial V/\partial T)_P>0$ so $(\partial S/\partial V)_T>0$, consistent with the positive slope of the LDL–HDL transition line $\mathrm{d}P/\mathrm{d}T$ (see Fig. 11). We confirm our expectation that $(\partial S/\partial V)_T>0$ by explicitly calculating S for our system by means of thermodynamic integration.

Our results show that the presence of two critical points and the occurrence of the density anomaly are not necessarily related, suggesting that one might seek experimental evidence of a liquid–liquid phase transition in systems with no density anomaly. In particular, a second critical point may also exist in liquid metals that can be described by soft-core potentials. Thus the class of experimental systems displaying a second critical point may be broader than previously hypothesized.

At some sets of parameters characterized by large $U_R=3U_A$, wide repulsive shoulder $(b=1.75a)$, and relatively narrow attractive well $(c=2.4a)$, we observe the development of the potential energy anomaly $\partial U/\partial V<0$. As we discuss above, this anomaly is a precursor of the density anomaly, which must develop if $\partial U/\partial V+P<0$. Hence, one may expect to find the density anomaly for isotropic potentials at wider repulsive shoulders and narrow attractive wells. However, we do not find the density anomaly even in the limiting case of a pure repulsive shoulder $(a=0,\ U_A=0,\ U_R=1,\ b=1)$. Note that the density anomaly was observed for 3D isotropic purely repulsive Gaussian potential [31–33] and for a soft-core potential with a repulsive ramp [45]. Hence the density anomaly in 3D may be sensitive to the details of the shape of the potential, such as the discontinuity in the double step potential (Fig. 2).

Acknowledgements

We wish to thank L.A.N. Amaral, V.V. Brazhkin, P.V. Giaquinta, T. Head-Gordon, E. La Nave, T. Lopez Ciudad, S. Mossa, G. Pellicane, N.V. Ryzhov, F.W. Starr, S.H. Stishov, J. Teixeira, and, in particular, F. Sciortino for helpful suggestions and discussions. We thank NSF for partial support.

References

[1] R. Waller, Essays of Natural Experiments [original in Italian by the Secretary of the Academie del Cimento, 1684], Johnson Reprint Corporation, New York, 1964.
[2] F.X. Prielmeier, E.W. Lang, R.J. Speedy, H.-D. Lüdemann, Phys. Rev. Lett. 59 (1987) 1128.
[3] F.X. Prielmeier, E.W. Lang, R.J. Speedy, H.-D. Lüdemann, B. Bunsenges, Phys. Chem. 92 (1988) 1111.
[4] L. Haar, J.S. Gallagher, G.S. Kell, NBS/NRC Steam Tables. Thermodynamic and Transport Properties and Computer Programs for Vapor and Liquid States of Water in SI Units, Hemisphere Publishing Co., Washington DC, 1984, pp. 271–276.
[5] P.G. Debenedetti, Metastable Liquids, Princeton University Press, Princeton, 1996.
[6] O. Mishima, H.E. Stanley, Nature 396 (1998) 329.
[7] Y. Yoshimura, B. Bunsenges, Phys. Chem. 95 (1991) 135 and references therein.
[8] P.H. Poole, F. Sciortino, U. Essmann, H.E. Stanley, Nature 360 (1992) 324–328.
[9] S. Harrington, R. Zhang, P.H. Poole, F. Sciortino, H.E. Stanley, Phys. Rev. Lett. 78 (1997) 2409; S. Harrington, P.H. Poole, F. Sciortino, H.E. Stanley, J. Chem. Phys. 107 (1997) 7443.
[10] F. Sciortino, P.H. Poole, U. Essmann, H.E. Stanley, Phys. Rev. E 55 (1997) 727.
[11] O. Mishima, Phys. Rev. Lett. 85 (2000) 334–336.
[12] M.-C. Bellissent-Funel, Nuovo Cimento 20 D (1998) 2107–2122.
[13] V.V. Brazhkin, E.L. Gromnitskaya, O.V. Stalgorova, A.G. Lyapin, Rev. High Pressure Sci. Tech. 7 (1998) 1129–1131.
[14] Y. Katayama, T. Mizutani, W. Utsumi, O. Shimomura, M. Yamakata, K. Funakoshi, Nature 403 (2000) 170–173.
[15] M.C. Wilding, P.F. McMillan, J. Noncryst. Solids 293 (2001) 357.
[16] V.V. Brazhkin, S.V. Popova, R.N. Voloshin, High Pressure Res. 15 (1997) 267–305.
[17] A.K. Soper, M.A. Ricci, Phys. Rev. Lett. 84 (2000) 2881–2884.
[18] D.J. Lacks, Phys. Rev. Lett. 84 (2000) 4629–4632.
[19] M. van Thiel, F.H. Ree, Phys. Rev. B 48 (1993) 3591–3599.
[20] J.N. Glosli, F.H. Ree, Phys. Rev. Lett. 82 (1999) 4659–4662.
[21] I. Saika-Voivod, F. Sciortino, P.H. Poole, Phys. Rev. E 63 (2001) 011202-1–011202-9.
[22] M.R. Sadr-Lahijany, A. Scala, S.V. Buldyrev, H.E. Stanley, Phys. Rev. Lett. 81 (1998) 4895–4898.
[23] M. Reza Sadr-Lahijany, A. Scala, S.V. Buldyrev, H.E. Stanley, Phys. Rev. E 60 (1999) 6714.
[24] A. Scala, M.R. Sadr-Lahijany, N. Giovambattista, S.V. Buldyrev, H.E. Stanley, Phys. Rev. E 63 (2001) 041202.
[25] G. Franzese, G. Malescio, A. Skibinsky, S.V. Buldyrev, H.E. Stanley, Nature 409 (2001) 692.
[26] S.M. Stishov, preprint.
[27] R.J. Speedy, J. Chem. Phys. 107 (1997) 3222–3237.
[28] P.C. Hemmer, G. Stell, Phys. Rev. Lett. 24 (1970) 1284; G. Stell, P.C. Hemmer, J. Chem. Phys. 56 (1972) 4274–4286.
[29] J.S. Høye, P.C. Hemmer, Physica Norvegica 7 (1973) 1.
[30] P.G. Debenedetti, V.S. Raghavan, S.S. Borick, J. Phys. Chem. 95 (1991) 4540–4551.
[31] F.H. Stillinger, D.K. Stillinger, Physica A 244 (1997) 358.
[32] F.H. Stillinger, T.A. Weber, J. Chem. Phys. 68 (1978) 3837.
[33] F.H. Stillinger, T.A. Weber, J. Chem. Phys. 74 (1981) 4015.
[34] K.K. Mon, N.W. Ashcroft, G.V. Chester, Phys. Rev. B 19 (1979) 5103; K.K. Mon, N.W. Ashcroft, G.V. Chester, J. Phys. F 15 (1985) 1215.

[35] M. Silbert, W.H. Young, Phys. Lett. 58 A (1976) 469–470.
[36] D. Levesque, J.J. Weis, Phys. Lett. 60 A (1977) 473–474.
[37] J.M. Kincaid, G. Stell, Phys. Lett. 65 A (1978) 131–134.
[38] P.T. Cummings, G. Stell, Mol. Phys. 43 (1981) 1267–1291.
[39] E. Velasco, L. Mederos, G. Navascués, P.C. Hemmer, G. Stell, Phys. Rev. Lett. 85 (2000) 122–125.
[40] A. Voronel, I. Paperno, S. Rabinovich, E. Lapina, Phys. Rev. Lett. 50 (1983) 247–249.
[41] T. Head-Gordon, F.H. Stillinger, J. Chem. Phys. 98 (1993) 3313.
[42] F.H. Stillinger, T. Head-Gordon, Phys. Rev. E 47 (1993) 2484–2490.
[43] A. Ben-Naim, Statistical Thermodynamics for Chemists and Biochemists, Plenum Press, New York, 1992, pp. 233–238 (See especially Fig. 4.9, p. 233).
[44] C.H. Cho, S. Singh, G.W. Robinson, Phys. Rev. Lett. 76 (1996) 1651.
[45] E.A. Jagla, Phys. Rev. E 63 (2001) 061501;
E.A. Jagla, Phys. Rev. E 63 (2001) 061509;
E.A. Jagla, J. Chem. Phys. 111 (1999) 8980.
[46] M. Canpolat, F.W. Starr, A. Scala, M.R. Sadr-Lahijany, O. Mishima, S. Havlin, H.E. Stanley, Chem. Phys. Lett. 294 (1998) 9.
[47] S.H. Behrens, D.I. Christl, R. Emmerzael, P. Schurtenberger, M. Borkovec, Langmuir 16 (2000) 2566–2575.
[48] S. Sastry, P.G. Debenedetti, F. Sciortino, H.E. Stanley, Phys. Rev. E 53 (1996) 6144.
[49] A. Skibinsky, S.V. Buldyrev, A. Scala, S. Havlin, H.E. Stanley, Phys. Rev. E 60 (1999) 2664–2669.
[50] M.P. Allen, D.J. Tildesley, Computer Simulation of Liquids, Oxford University Press, New York, 1989.
[51] D.C. Rapaport, The Art of Molecular Dynamic Simulation, Cambridge University Press, Cambridge, 1995.
[52] B.J. Adler, T.E. Wainwright, J. Chem. Phys. 31 (1959) 459–466.
[53] B.D. Lubachevsky, J. Comput. Phys. 94 (1991) 255–283.
[54] A.Yu. Grosberg, A.R. Khokhlov, Giant Molecules, Academic Press, London, 1997.
[55] N.V. Dokholyan, S.V. Buldyrev, H.E. Stanley, E.I. Shakhnovich, J. Mol. Biol. 269 (2000) 1183–1188.
[56] R.J. Speedy, J. Chem. Phys. 114 (2001) 9069–9074.
[57] R.J. Speedy, Mol. Phys. 95 (1998) 169–178.
[58] H.J.C. Berendsen, J.P.M. Postma, W.F. van Gunsteren, A. DiNola, J.R. Haak, J. Chem. Phys. 81 (1984) 3684–3690.
[59] A. Scala, M. Reza Sadr-Lahijany, N. Giovambattista, S.V. Buldyrev, H.E. Stanley, J. Stat. Phys. 100 (2000) 97.
[60] E.A. Jagla, Phys. Rev. E 58 (1998) 1478.
[61] A. Scala, F.W. Starr, F. Sciortino, E. La Nave, H.E. Stanley, Nature 406 (2000) 166.
[62] G. Adam, J.H. Gibbs, J. Chem. Phys. 43 (1965) 139.
[63] C. Caccamo, Phys. Rep. 274 (1996) 1–105.
[64] P. Rein ten Wolde, D. Frenkel, Science 277 (1997) 1975–1978.
[65] M.H.J. Hagen, E.J. Meijer, G.C.A.M. Mooij, D. Frenkel, H.N.W. Lekkerkerker, Nature 365 (1993) 425–426.